POLITECNICO
MILANO 1863

SCUOLA DI INGEGNERIA INDUSTRIALE
E DELL'INFORMAZIONE

EXECUTIVE SUMMARY OF THE THESIS

Experimental investigation of microfibers dispersion in fully developed turbulent channel flow

TESI MAGISTRALE IN MECHANICAL ENGINEERING – INGEGNERIA MECCANICA

AUTHOR: SILVIA SAMBUCA

ADVISOR: GIANLUCA MONTENEGRO

CO-ADVISOR: ALFREDO SOLDATI

ACADEMIC YEAR: 2021-2022

1. Introduction

Fully developed channel flow has been studied extensively for almost a century now to increase the understanding of the mechanics of wall bounded turbulent flows through either direct numerical simulations (DNS) and/or experimentally. Despite the large amount of documentation being available and the relatively simple flow, up to nowadays there is still poor agreement among the reported measurements, even in low-order statistics as the turbulence intensities, especially in the vicinity of the wall. In addition, only a few statistical quantities or physical mechanism of turbulence flows are recognized as universal, so this means that a basic understanding of the entire flow field is not yet totally reached, which is needed in order to improve the engineering of vehicles and transport systems that society heavily depends upon at this point in time [(Monty & Chong, 2009)]. In addition to the study of wall bounded turbulence, this work is committed into the investigation of non-axisymmetric microfibers in a turbulent channel flow. The study of these anisotropic particles is of particular interest for both industrial and environmental applications [(Voth & Soldati, 2017)]. The aim of this thesis is therefore:(1)the investigation of turbulence in a turbulent channel flow configuration carried out in the TU Wien Turbulent Water Channel (schematized in the Figure 1-1) through turbulence statistics derived from 2D Particle Image Velocimetry measurements;(2)the study of the geometrical

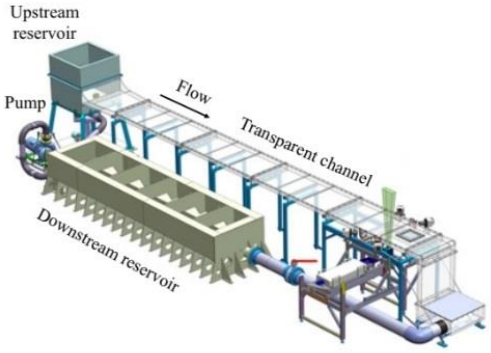

Figure 1-1: Schematic of the TU Wien Turbulent Water Channel.

properties of the plastic microfibers in the water channel reconstructed by employing in-house built MATLAB codes by using images coming from acquisition system.

2. Experimental set-up

For this thesis then a total of two sets of three experiments each were performed, conducted at 180,360 and 720 friction Reynolds distinguishing among unladen and fiber laden flows. The experimental facility for both flow configurations is the TU Wien Turbulent Water Channel, consisting of a 10m long water channel, constructed by combining five sections of 2 metres each, with cross-sectional dimensions of 80 cm x 8 cm (w x 2δ, where δ indicates the half-channel height).The images were recorded in correspondence of the test section, located 8.5 m downstream of the channel entrance, using one high speed camera (Phantom VEO 340 L with CMOS sensor with sensor size of 2560 x 1600 pixels at 0.8 kHz) placed to have the objective lens with an angle of 90° with respect to the lateral walls of the channel. The measurement volume is located mid-span of the channel and illuminated by a thick laser sheet (Litron LD60-532 PIV). Data acquisition has been performed using single frame method with different frequencies of acquisition differentiating between unladen and fibers laden flows (camera settings and measured quantities are given in Table 2.1 and Table 2.2 for unladen and fiber laden flows respectively).

Re_τ	T_i	T_f	Acq. f	f#	M
[-]	[°C]	[°C]	[KHz]	[-]	[-]
200	22.95	22.70	0.4	16	0.25
340	23.15	23.07	0.8	16	0.25
650	23.39	23.28	1.3	16	0.25

Table 2.1: Camera recording parameters adopted and relevant measured quantities.

Re_τ	T_i	T_f	Acq. f	f#	M
[-]	[°C]	[°C]	[KHz]	[-]	[-]
187	24.04	24.25	1	8	0.25
368	23.68	23.99	1	8	0.25
726	23.28	23.97	1	8	0.25

Table 2.2: Camera recording parameters adopted and relevant measured quantities.

where Ti and Tf are the initial and final temperature measured by the temperature sensor, acq. f is the acquisition frequency, M is the magnification and f# the f-number of the camera.

3. Unladen flow

From the acquired unladen flow images, the optic technique of PIV was used to carry out the measurements for the velocity fields. The way in which PIV obtains the velocity of the fluid is through the tracer particles velocity. The channel was therefore seeded with neutrally buoyant tracers with a diameter of 20 μm. The initial raw images were cutted to eliminate the noise due to the reflection of the glass (the images were cutted at the wall) and redundant information on the x direction (raw image displayed in Figure 3-1).

Figure 3-1: Cutted raw image.

PIV measurements were conducted using PIVlab from MATLAB. The squared windows sizes and time resolutions chosen are D_I=8,16,24 and 32 pixels and dt=(4,6,8);(2,3,4) and 1ms for Re_τ=187, 368 and 736 respectively: resulting in twelve combinations for low and intermediate Reynolds numbers and four for high Reynolds number. Different time resolutions were obtained for lower and intermediate cases through image shifting technique: it consists in skipping an arbitrary number of frames with the aim of obtaining larger particles' displacements and reduce the uncertainty of PIV measurements.

3.1. Uncertainty of PIV

To guarantee accurate turbulence measurements, the measurement area in which each velocity vector is estimated must be small compared to the

smallest size of turbulent structure. [(Scharnowski & Kähler, 2019)].

Re_τ	η	τ_η
[-]	[μm]	[ms]
187	792.6	690.3
368	480	251.1
726	272.7	81.5

Table 3.1: Kolmogorov scales for unladen flow experiments.

[pixels]	8	16	24	32
[μm]	325.6	651.2	976.8	1302.5

Table 3.2: Window's dimensions in metric scale.

In Table 3.1 the values for the Kolmogorov length and time scales for the unladen flow experiments are given. For a better readability and comparison, Table 3.2 the dimensions in pixels of the interrogation windows are given in μm using a scaling factor equal to 0.0407 mm/pixel (obtained from the calibration). From the comparison between tables, it is clear that the dimensions of the squared IWs (i.e., interrogation windows) are lower than the smallest of the turbulence structure sizes, except for one case: 8x8 window applied on the experiment with Re_τ=726.

PIV measurement uncertainty is also related to window size and time resolution choices: the combination of lowest window size and dt (lower displacement of the image particle) gives an amplified noise in the result. For increasing particle displacement as for increasing window size D_I the velocity field is much smoother and thus better suited for turbulence estimations. On the other hand, increasing dt or the IW's size could lead to too smoothed results which might filter out small-scale turbulence structures.

One important systematic error source that was then analysed for PIV uncertainty is peak locking. According to Raffel (Raffel, et al., 2018), the continuous intensity distribution of very small particle images is insufficiently sampled by the discrete digital camera sensor. Thus the estimated displacements are shifted toward the closest integer pixel positions and, as a results, the velocity is over- or underestimated depending on the sub-pixel length of the shift vector in the image plane. To examine the presence of peak-locking it is possible to inspect the probability density function of the displacement (in pixels) of the particle [(Christensen, 2004)]. This was done for all the time and spatial resolutions investigated, but here for the sake of briefness only one window size (i.e., 16 pixels) for only one case of Reynolds number (Re_τ=368) is shown (the bin sizes for the determination of the probability density function was 0.1 pixel). From Figure 3-2 it's clear that peak-locking is mostly affecting only the smallest time resolution. But also in the worst-case PDF seems well distributed for all the values, also in between the integers.

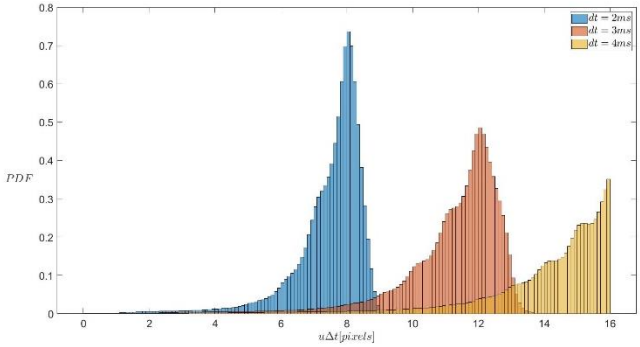

Figure 3-2: PDF of particle-image displacement.

4. Fiber laden flow

From the acquired images in the case of fiber laden flow (flow is seeded with tracers and fibers) it was possible to perform the discrimination and modeling of the fibers to extract geometrical properties. through in-house built MATLAB codes. Among all the experiments, it was decided to perform the reconstruction only for the case of Re_τ=200, with the objective of creating a flexible in-house code applicable for all Re_τ cases.

4.1. Discrimination phase

The first step was to distinguish the fibers from the tracers and other possible spurious objects. As a first step the recorded images were pre-processed using the commercial software Lavision GmbH: Davis 10.2. After the pre-processing, the images were as the one displayed in Figure 4-1 (notice that in the image the contrast was purposely increased to show it more clearly).

From the figure it appears clear how the fibers are well recognizable from their elongated shape and being them larger in size with respect to the tracers leads for them to scatter more light, implying that

the intensities reached by the fibers are higher. For the discrimination so intensity and area thresholds were applied to the raw images, which values were decided arbitrary by the observation of the available raw images coming from the experiments (Intensity threshold was set to 300 and for the upper bound and lower bound Area thresholds were set to 200 and 50 pixels respectively).

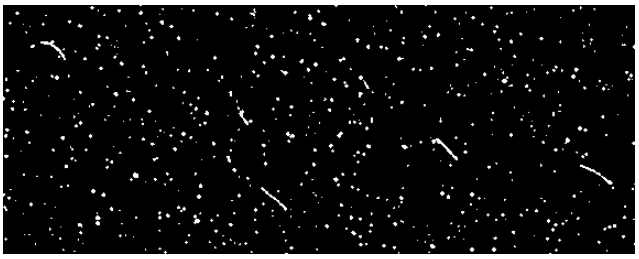

Figure 4-1: Group of fibers in a zoomed pre-processed image.

4.2. Modeling Phase

After the discrimination each fiber must be associated with the representing global coordinates in the two-dimensional image. Using the built-in command *regionprops* on MATLAB, it was possible to obtain for each particle image identified as a fiber a set of information as area, centroid, major and minor axes length and orientation. From observations of the fibers in dry conditions and from the model's choice used in the literature [(Alipour, 2021)], it was possible to conclude that the function that best fits in a least-square sense the single fiber is a 2nd order polynomial. According to the orientation three methods were proposed for the definition of the polynomial. Before applying the methods for the approximation of the best fitting polynomial, the application of a 2D Gaussian smoothing filter with a suitable kernel was necessary.

When the orientation of the fiber is lower than 45° (targeted as a horizontal fiber) than the model searches for the intensity peaks along the first dimension (i.e., along the columns, so vertical cutting method) which are expected to be at the centroids of the fiber otherwise peaks are searched on the second dimension (i.e., along the rows).

In Figure 4-2 the methods are compared: a third one was investigated too, in which the maximum intensity was searched in a "moving" 5x5 matrix. Nevertheless, this strategy was rejected in favor of the simpler model of vertical cutting, since they gave similar results.

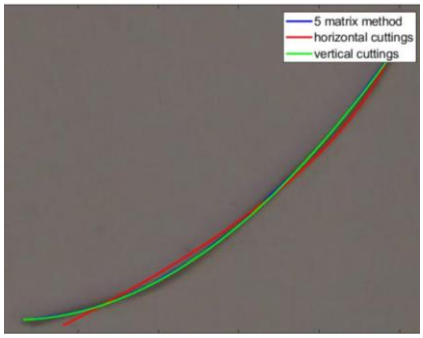

Figure 4-2: Case of a 45° oriented fiber.

5. Results for fibers

The fibers used in this study can be considered as slender body particles having high length-to-diameter ratio (λ=120) and a manufactured nominal length L_f=1.2 mm. From their reconstruction, it was possible to derive other properties such as length L_f, effective length L_{eff} and curvature k: where L_{eff} is defined as the distance between the two ends of the fiber (for straight fibers it coincides with L_f). Latter can be calculated as the length of an arc as depicted in Equation (5.4).Limits a and b define respectively the x coordinates of the starting and end point of the fiber and y the coordinates of the 2nd order polynomial used to approximate the fiber).

$$\mathbf{L_f} = \int_a^b \sqrt{1 + \left(\frac{dy}{dx}\right)^2}\, dx\,; \qquad (5.1)$$

To evaluate the curvature k, first the local curvature k_l must be defined as in Equation (5.2):

$$\boldsymbol{k_l} = \frac{|y''|}{(1+y'^2)^{3/2}}\,; \qquad (5.2)$$

Finally, the curvature k can be obtained as in Equation (5.3):

$$\boldsymbol{k} = \frac{1}{L_f}\int_a^b |k_l| dx; \qquad (5.3)$$

The length of the reconstructed fibers can be calculated by computing the Probability density

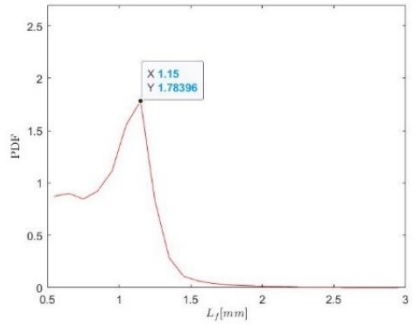

Figure 5-2: PDF of fibers lengths.

function of the length (Figure 5-2) of all the fibers reconstructed in the experiment and the representative length is chosen to be the peak of the PDF (L_f=1.15 mm) which is slightly lower than the one nominal one, but still acceptable.

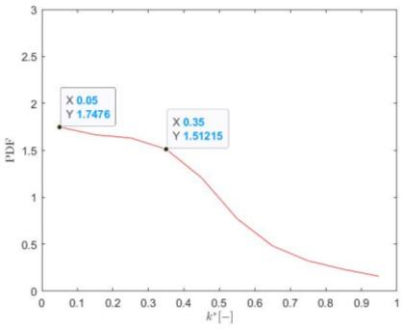

Figure 5-1: PDF of the normalized curvature.

For the curvature, k* was considered: defined as mean curvature k normalized by k_0, which is calculated as the curvature of an arc of half circle with length equal to the mean length of the fibers (i.e., $k_0=\pi/\bar{L}_f$). In this way fibers can be classified according to two limits: if k* is 0 valued, then the fiber can be considered straight, otherwise if k*=1 then the fiber is semi-circumference shaped. From the PDF of curvature (Figure 5-1), it's clear the presence of errors introduced in the discrimination phase. Indeed, the PDF shows a low peak at k*=0.05 (almost straight fibers) which is most probably due to two types of errors: either the reconstruction was not able to detect the real curvature of the fiber due to the presence of close particles or a cluster of particles was mistaken as a single fiber. It is however interesting to see how k*=0.35 (same value resulted from Alipour analysis) is however still a local maximum for the PDF obtained from the current study.

Finally, assuming that the fiber is part of a circumference, the L_{eff} can be calculated analytically by knowing k using the following correlation:

$$\boldsymbol{L_{eff}} = \frac{\sqrt{(2-2\,cos(kL_f))}}{k}; \qquad (5.4)$$

So it was interesting to show the distribution of normalized curvatures and effective lengths of the fibers available in this study (Figure 5-3).After the analytical prediction (black dashed curve in figure) was plotted: the curve was obtained substituting $k=k_0 \cdot k^* = \pi/\bar{L}_f k^*$ in Equation (5.4). It can be observed that the distribution is quite symmetric with respect to the analytical predictions and mostly the fibers examined in this thesis are concentrated at the top and left part of the length and curvature ranges respectively.

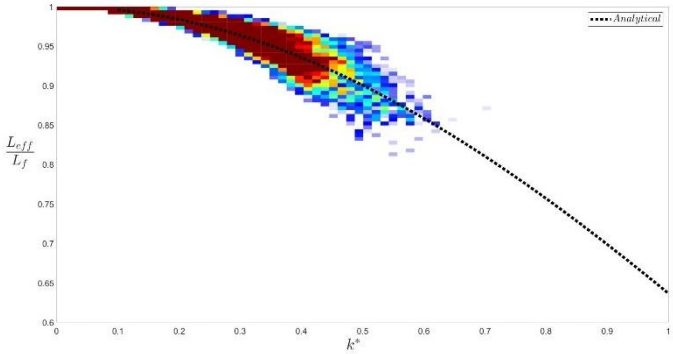

Figure 5-3: Joint PDF of L_{eff} and k*.

6. Turbulence statistics

The results on the turbulence statistics can be obtained. So firstly, for each of the three Reynolds numbers the first and second order statistics were studied. Also, higher order moments (i.e., skewness and flatness) of velocity fluctuations were evaluated to discuss and quantify the non-Gaussian and intermittent behaviour of the turbulence structures. Finally, the universality of near wall turbulence in the channel was examined in the limits of the available data. For the seek of clarity it was chosen to show for this executive summary only the results from one of the three Reynolds (i.e., Re_τ=187).

$Re_{\tau,eff}$	u_τ	τ	δ_v
[-]	[m/s]	[s]	[mm]
187	0.0043	0.0503	0.214

Table 6.1: Wall scales for Re_τ=187.

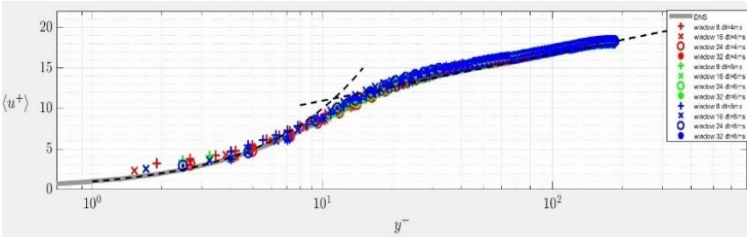

Figure 6-1: Mean velocity profiles.

The profile of the mean streamwise velocity non-dimensionalized by the wall-shear velocity u_τ (defined in Table 6.1) is shown in Figure 6-1. In the figure the profile coming from DNS of Moser for Re_τ=180 [(Moser, Kim, & Mansour, 1999)] is depicted in grey and in black the theoretical laws of the wall and the log wall are represented. In general, all time resolutions and window sizes bring good results: one of the best set up among all the choices is D_I=24 pixel with the smallest and intermediate dt (i.e., dt=4,6 ms). For low size IW the resolution is very high and we were able to measure at very low wall units ($y^+ \approx$ 1-2).
Later the r.m.s. of the fluctuations normalized by u_τ are calculated: it's interesting to notice how turbulent channel flow is characterized by higher u' at wall unit y^+<20, presenting a peak at around $y^+\approx$12 and the normal component of the velocity fluctuations shows values of an order of magnitude lower than the one of the streamwise component near the wall. Therefore v' is also much more affected by spatial and time resolutions. For the right combination of dt and D_I, also the turbulence intensities from our measurements follow the DNS data from literature.

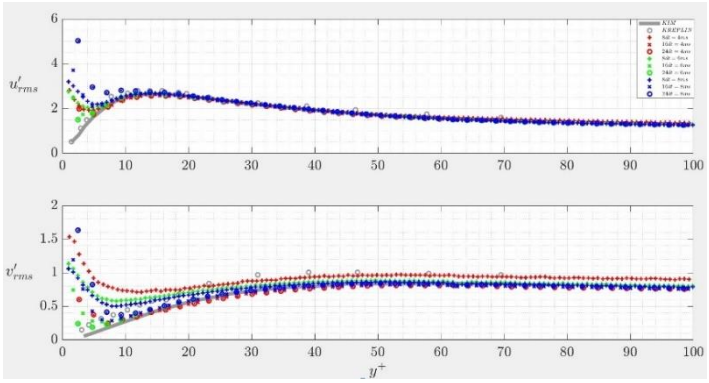

Figure 6-2: R.m.s velocity fluctuations normalized by u_τ.

For the Reynolds stresses the discussion is analogous, discrepancies are detected in the near-wall region and tend to 0 in the outer region and far from the wall. Best fitting was found for dt=6ms. Finally, the higher order statistics are analyzed. The profiles computed in this work were able follow the data coming from literature and were able to highlight (better than the other experimental data) the non-Gaussian behavior of turbulence especially near the wall.

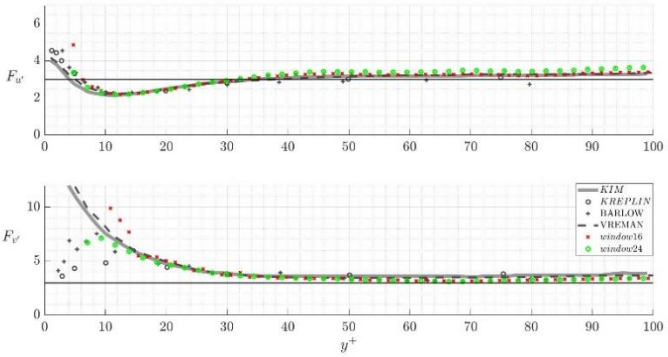

Figure 6-3: Flatness of turbulence fluctuations.

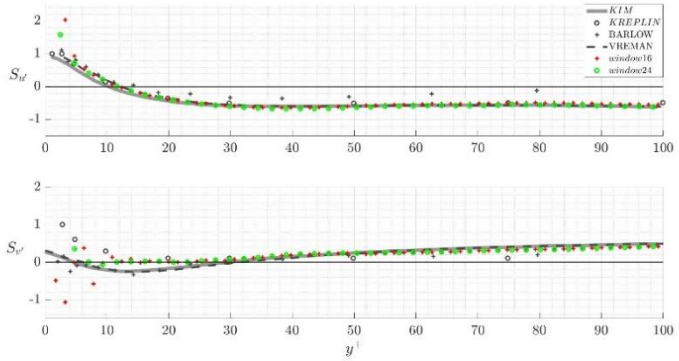

Figure 6-4: Skewness of turbulence fluctuations.

The universality of turbulence near the wall (normalized in wall scales) was checked with the available database created in this thesis. While for the mean streamwise velocity, a similar behavior as the one described in literature was found, nothing could be concluded for fluctuations and Reynolds stresses, due to the low resolution for the higher Re_τ case close to the wall.

7. Conclusions

From PIV measurements of the instantaneous velocity fields (in the streamwise and normal directions) it was possible to assure the flow quality of TU Wien Turbulent Water Channel with the study of turbulence statistics so to guarantee for future studies to work in statistically fully developed channel flow. Other than that, it was possible to perform a data supported discussion on the uncertainty of the PIV measurements in developing this analysis by comparing the obtained results with the direct numerical simulations and experimental data from literature. Latter is much relevant considering that future projects will be conducted in the studied water channel using PIV technique: therefore, this thesis is proposed as a starting database and lays the groundwork for future works employing PIV technique in TU Wien Turbulent Water Channel. The results show that the turbulence statistics followed the trends available in the literature: for the right combination of time resolution dt and window size D_I, especially at low and moderate Re_τ, the results are good also for skewness and flatness of fluctuations, for which scarce or none experimental data is available in the literature at the moment. Finally, the still uncertain universality of turbulence near the wall was investigated in the limitation of the data obtained in this work: for the mean velocity the trends appear similar to one observed for higher Reynolds in the literature, instead not much can be concluded on higher order statistics. Despite the very small discrepancies for which different explanations were given in the thesis, the configuration was assured to be statistically a fully developed channel flow and we were able to demonstrate that PIV is an efficient tool to study turbulence near and far from the wall. It was indeed able to arrive at very small y^+ (microscales) compared to the experimental data in the literature, despite the presence of reflections of the glass and other sources of error that occur near the wall. In addition to that, also a method for the reconstruction of microplastics fibers in the water channel from planar PIV measurements was proposed. Indeed, in the optic of future study on the dynamic of fibers through PIV technique, a preliminary reconstruction of the fibers from the images is needed in order to detect their position and therefore their motions and rotations during the experiments. Through the reconstruction, also properties as the length and the curvature were derived representing a step forward for the characterization of complex objects in turbulent channel flows. There are various topics of interest that could be tackled in the future based on the methodology used in this thesis for the reconstruction of the fibers: 3D PIV measurements of microplastic fibers in turbulence water channel, PTV measurements in water channel and so on. In fact, the methodology proposed in this thesis has the flexibility to be implemented in different flow boundary conditions and fiber properties.

8. Bibliography

Alipour, M. (2021). *Orientation and rotation rates of non-axisymmetric fibers in turbulent channel flow.* Doctoral thesis, Technische Universität Wien, Institute of Fluid Mechanics and Heat Transfer.

Christensen, K. T. (2004). The influence of peak-locking errors on turbulence statistics computed from PIV ensembles. *Experiments in Fluids, 36*, 484-497. doi:10.1007/s00348-003-0754-2

Monty, J., & Chong, M. (2009). Turbulent channel flow: Comparison of streamwise velocity data from experiments and direct numerical simulation. *Journal of Fluid Mechanics, 633*, 461-474. doi:10.1017/S0022112009007769

Moser, R. D., Kim, J., & Mansour, N. N. (1999). Direct numerical simulation of turbulent channel flow up to Ret=590. *Physics of fluid, 11(4)*, 943. doi:https://doi.org/10.1063/1.869966

Raffel, M., Willert, C. E., Fulvio, S., Kähler, C. J., Wereley, S. T., & Kompenhans, J. (2018). *Particle Image Velocimetry.* Switzerland: Springer.

Scharnowski, S. B., & Kähler, C. (2019). Accurate turbulence level estimations using PIV/PTV. *Experiments in Fluids, 60(1).* doi:10.1007/s00348-018-2646-5

Voth, G. A., & Soldati, A. (2017). Anisotropic Particles in Turbulence. *Annual Review of Fluid Mechanics, 49*, 249-276 . doi:10.1146/annurev-fluid-010816-060135